International Journal of Nanomedicine

Dovepress

open access to scientific and medical research

Open Access Full Text Article

ORIGINAL RESEARCH

The Combined Effect of Nanobubble-IR783-HPPH-Affibody Complex and Laser on HER2-Positive Breast Cancer

Wenbin Cai[1,2,*], Wei Lv[1,3,*], Li Meng[2], Yunyou Duan[1], Li Zhang[1]

[1]Department of Ultrasound Medical, Tangdu Hospital, the Fourth Military Medical University, Xi'an, People's Republic of China; [2]Department of Ultrasound Diagnostics, General Hospital of Tibet Military Region, Lhasa, People's Republic of China; [3]Department of Radiology, 305 Hospital of Chinese People's Liberation Army, Beijing, People's Republic of China

*These authors contributed equally to this work

Correspondence: Li Zhang, Department of Ultrasound Medical, Tangdu Hospital, 569# Xinsi Road, Baqiao District, Xi'an, People's Republic of China, Tel +86-29-84777171, Fax +86-29-83510181, Email lilyzhang319_20@hotmail.com

Introduction: Nanobubble is an innovative ultrasound contrast agent that triggers the development of targeted imaging of HER2-positive breast cancer by combining with HER2 affibody and IR783. HPPH is a second-generation photosensitiser that is effective in treating tumours. Hence, the nanobubble-IR783-HPPH-affibody (NIHA) complex demonstrates considerable potential in the treatment of HER2-positive breast cancer.

Methods: We fabricated the NIHA complex via an advanced thin-film hydration method and detected its characteristics such as particle size, morphology, stability, and cytotoxicity. Moreover, the effect of NIHA complex with laser on HER2-positive breast cancer was confirmed via in vitro and in vivo experiments.

Results: The NIHA complex was spheroid, stable and exhibited no cytotoxicity; moreover, its particle size was 524.8 ± 53.3 nm (n = 5). In combination with laser treatment, NIHA complex reduced the cell viability and tumour volume, induced apoptosis of HER2-positive breast cancer cells, and prolonged survival of nude mice.

Conclusion: The newly prepared NIHA complex with laser treatment has the potential on treating HER2-positive breast cancer.

Keywords: HER2, breast cancer, HPPH, nanobubbles, laser

Introduction

Breast cancer is the third most common type of cancer and is the leading cause of cancer-related deaths among females worldwide.[1] Human epidermal growth factor receptor 2 (HER2), a 185-kDa transmembrane tyrosine kinase protein, is amplified or overexpressed in approximately 20% of breast cancers, which is called HER2-positive breast cancer.[2] HER2-positive breast cancer exhibits a poor prognosis, high mortality rates,[3,4] and demonstrates resistance to tamoxifen[5,6] and an increased risk of brain metastases.[7] With continuous efforts engaged in the development of therapy and in the improvement of patient care, particularly in the application of trastuzumab, disease-free survival and overall survival are improved in HER2-positive breast cancer patients[8,9]; however, some patients still have to undergo some posers such as relapse, disease progression within 1 year, and intrinsic or acquired resistance and so forth.[10] Therefore, non-invasive and targeted treatment of HER2-positive breast cancer with low side effects remains challenging.

Photodynamic therapy (PDT) is a non-invasive and innovative method for cancer therapy, which has been widely used in the studies and management of malignant lesions.[11] PDT, which involves three basic elements, namely photosensitizer, oxygen, and light,[12] can generate reactive oxygen species (ROS) by exposing photosensitizers to a specific wavelength of light to inflict irreversible damage on the tumour cells.[13] With the development of the second-generation photosensitizers, the limitations such as difficulty in synthesis, poor tissue penetration, and

Received: 24 August 2022
Accepted: 9 January 2023
Published: 19 January 2023

prolonged cutaneous photosensitivity[14] have been overcome. Notably, 2-[1-hexyloxyethyl]-2-devinyl pyropheophorbide-a (HPPH) is the most effective agent and exhibits more optimal photophysical properties, higher accumulation in tumour, and mild skin photosensitivity.[15,16] Targeting HPPH delivery system is the point.

Nanobubble (NB), a novel ultrasound contrast agent, has demonstrated the potential to be used in molecular and targeted imaging in numerous diseases, particularly cancer. Compared to the conventional ultrasound contrast agent microbubble (MB) whose size is 1–10 μm, NB is preferred due to its nano-size to extravasate through the vascular wall into the extravascular space via the enhanced permeability and retention (EPR) effect of tumour tissue[17–20] what MB is incapable,[21] which is called passive targeting.[22] Moreover, NB could be modified with active targeting agent such as affibody, capable of HER2 molecule recognition and IR783, a near-infrared fluorescent dye, capable of cancer cell–specific binding, which strengthened its targeting ability in our previous studies.[23,24] The characteristics of NB enable itself not only as an ultrasound contrast agent to perform target imaging but also an optimal carrier to deliver therapeutic agent for cancer.

In the present study, we fabricated the nanobubble-IR783-HPPH-affibody (NIHA) complex, utilised its nano-sized features, and the ability of targeting improved accumulation of HPPH in breast cancer (Figure 1); with laser the complex inhibited tumour growth and provided experimental support for the non-invasive and targeted treatment of HER2-positive breast cancer.

Methods

Materials

The phospholipids 1,2-distearoyl-*sn*-glycero-3-phosphoethanolamine-N-[biotinylated(polyethyleneglycol)–2000] (biotinylated DSPE-PEG [2000]; MW, 3016.781 g/mol) and 1.2-dipalmitoyl-*sn*-glycero-3-phosphocholine (DPPC; MW, 734.039 g/mol), were purchased from Avanti Polar Lipids Inc (USA) in a powdered form without further purification, and were used to fabricate nanobubbles. Near infrared fluorescent agent IR783 was purchased from Sigma-Aldrich (St. Louis, MO). 2-(1-Hexyloxyethyl)-2-devinyl pyropheophorbide-a (HPPH) was purchased from Shanghai

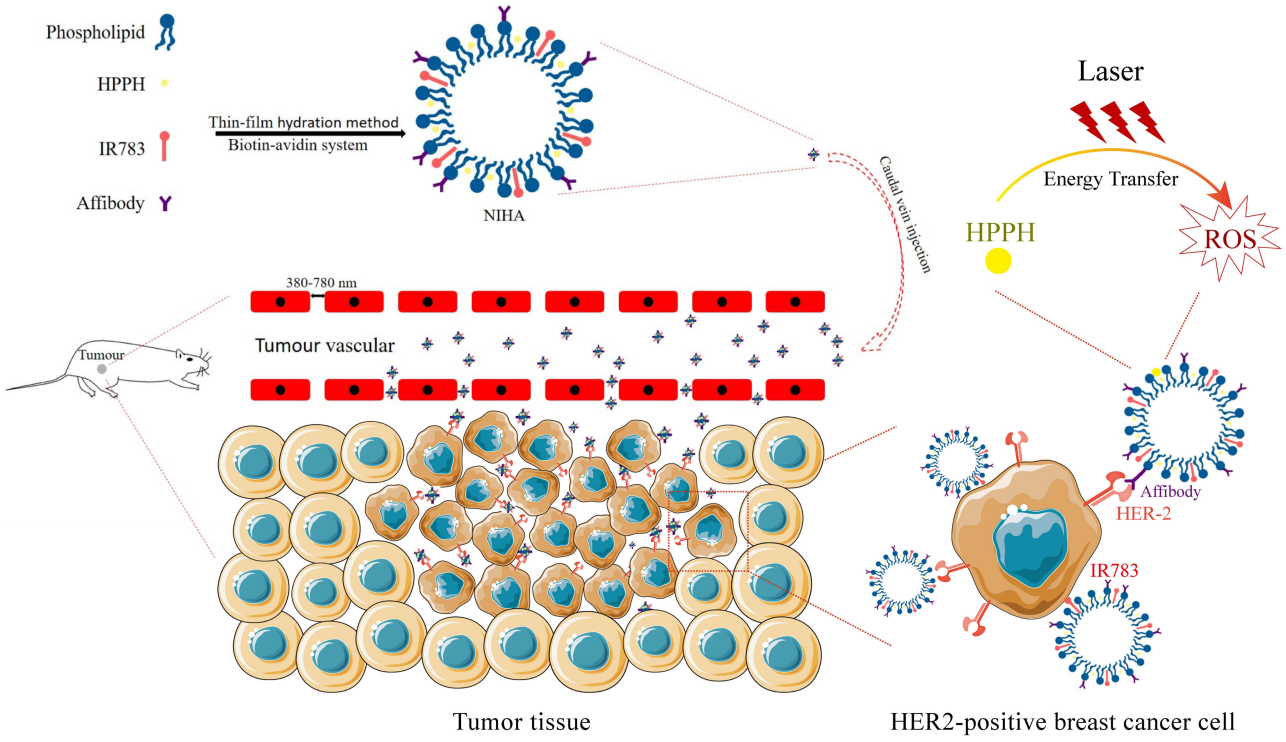

Figure 1 Schematic diagram of the nanobubble-IR783-HPPH-affibody (NIHA) complex formation and behaviour in the tumour tissue. The NIHA complex penetrates the blood vessel of the tumour tissue and target specific HER2-positive cancer cells and killed the cancer cells via ROS effect under laser exposure.

AZBIOCHEM Co. Chloroform was purchased from Kehao Co. ImmunoPure® streptavidin was purchased from Pierce (Rockford, IL). Biotinylated anti-ErbB2 Affibody® was purchased from Abcam (USA). The BT-474 cell line and the MDA-MB-231 cell line were purchased from the American Type Culture Collection (USA). The Cell Counting Kit-8 (CCK-8) kit was purchased from Dojindo Laboratories, Kumamoto (Japan).

Fabrication of the Nanobubble-IR783-HPPH-Affibody Complex

The nanobubble-IR783-HPPH-affibody (NIHA) complex was fabricated via improved thin-film hydration method, consistent with the protocols described in our previous study.[23–25] In a 25-mL rotary evaporation bottle, 14 mg DPPC and biotinylated DSPE-PEG (2000) with fixed ratio were added and 2 mL chloroform was used to dissolve them. Thereafter, 200 μL IR783 solution (1 mg/mL) and 200 μL HPPH solution (1 mg/mL) were added. After shaking the bottle evenly, the bottle was moved into a rotary evaporator and evaporation was performed at 120 rpm and 55 °C. After evaporation of chloroform, a phospholipid thin film was observed on the rotary evaporation bottle wall. Next, 1 mL of a hydration liquid comprising 10% glycerol and 90% 1 × phosphate-buffered saline (PBS) (V/V) was added into the bottle, and the bottle was transferred into an incubator shaker at 130 rpm and 37 °C for 60 min. Thereafter, the suspension formed was equally divided into two tubes covered by plastic caps. C_3F_8 gas was added to replace the air in the sealed tube. Each tube was oscillated for 45s in an amalgamator, and the bubble suspension in each tube was separately diluted to 8 mL with PBS. The nanobubble-IR783-HPPH suspension was then sterilised via CO_{60} irradiation.

Approximately 100 μL nanobubble-IR783-HPPH suspension, 850 μL PBS, and 100 μL streptavidin (concentration 10 mg/mL) were added and mixed in a tube. The tube was placed in mini-tube rotators and subjected to oscillation for 30 min at 18 rpm. Thereafter, the biotinylated anti-ErbB2 Affibody® molecules (50 μL, 1 mg/mL) were added into the suspension, and the mixture was centrifuged. The precipitate of streptavidin and excess affibody was removed with PBS three or four times. Eventually, the NIHA complex was formed after washing.

Characteristics of NIHA

The particle sizes of the nanobubble-IR783-HPPH complex and the NIHA complex were tested via dynamic light scattering (DLS). Meanwhile, the PDI (polydispersity index) and zeta potential of NIHA complex were tested on the DLS.1 mL sample, which was immediately measured after complete fabrication at 25 °C, and the experiment was repeated five times.

A transmission electron microscope (TEM) was used to visualise the morphology of the NIHA complex. A drop of the NIHA complex suspension was dropped onto a dust-free foil. It was placed in a desiccator and gold sputter-coated for 5 min, and then examined via TEM.

Optical imaging of the NIHA complex was performed by using a confocal laser scanning microscope (CLSM). A drop of sample was placed in a confocal culture dish and observed with excitation at 640 nm and peak emission at 780 nm.

The changes in particle size and concentration of the NIHA complex over time were assessed to determine stability. The particle size was tested as per the methods described above. The sample was added as a droplet on a haemocytometer and detected via fluorescence microscopy using a 100 × oil-immersion objective lens to measure concentration. The particle size and the concentration were measured at 1 min, 30 min, 60 min, 6 h, and 24 h after fabrication and the procedure was repeated five times.

The cytotoxicity of DPPC and DSPE-PEG was assessed in the previous study,[25] so the cytotoxicity of IR783 and HPPH was assessed via Cell Counting Kit-8 (CCK-8) assays in the present study. Briefly, HER2-positive breast cancer line BT-474 human breast cancer cells were seeded into 96-well plates at a density of 5000 cells/well and 100 μL/well of the cell culture medium, including the Dulbecco's modified Eagle medium (DMEM), with 10% fetal bovine serum (FBS) was added, after which the cells were cultured in a humidified atmosphere of 5% CO_2 and 37 °C. After 24 h, the medium was replaced with a fresh medium containing various concentrations of IR783 (1–40 μg/mL) and HPPH (0.15–40 μg/mL) respectively. After 24 h of culture, 10 μL of the CCK-8 reagent was added into each well. Eventually, after 4 h, the absorbance for each well was measured at 450 nm.

Tumour Cell Targeting Ability

The tumour targeting ability of the NIHA complex was evaluated via CLSM. The control group NB-HPPH was prepared in a manner similar to that of the NIHA complex without IR783 and affibody, which could be used to target cancer cells. 8 μL fluorescent dye Dil (1.2 mg/mL) was added to locate NB-HPPH. BT-474 cell was cultured in confocal culture dishes. Thereafter, 1 mL NIHA complex and NB-HPPH were added into dishes separately. After 30 min, the cells were subjected to washing steps thrice with PBS and incubated with 4% formaldehyde (1 mL) for 15 min. Next, 1 mL 0.1% Triton X-100 was added at room temperature for 10 min and then washing steps were performed with PBS. Furthermore, 1 μg/mL DAPI (4',6-diamidino-2-phenylindole) was added to perform staining of the nucleus, and after 5 min of incubation, the cells were subjected to washing steps thrice via PBS. Eventually, the cells were observed using CLSM.

The Effect of NIHA Complex with Laser on Cell in vitro

This experiment comprised four groups. 1) The NIHA-laser group: the cells were incubated with the NIHA complex (200 μL with concentration of 12×10^6) and medium for 30 min and subjected to washing steps with PBS. As reported,[26] a laser of 665 nm and 150 J/cm^2 was used. 2) The NIHA group: the cells were incubated with the NIHA complex (200 μL with concentration of 12×10^6) and medium for 30 min and subjected to washing steps with PBS, without laser. 3) The laser group: the cells were subjected to irradiation using a laser of 665 nm and 150 J/cm^2. 4) The control group: no processing was performed. The CCK-8 assay was conducted to evaluate cell viability. HER2-positive breast cancer cells BT-474 were seeded into 96-well plates at a density of 5000 cells per well. After 24 h of culture, the four groups were processed separately as described above. Next, 10 μL of the CCK-8 solution was added into each well after 48 h. Thereafter, the cells were incubated for 4 h and the absorbance at 450 nm in each well was measured by using the Infinite F200 Multimode plate reader. The cell viability was measured and expressed as (A1-A2)/(A3-A2) × 100%, where A1 represents the absorbance of well of each experimental group, A2 represents the absorbance of well with the medium and CCK-8 solution, and A3 represents the absorbance of well comprising the medium, CCK-8 solution, and cells. The test was repeated three times. Annexin-V was used to evaluate cell apoptosis. Briefly, 48 h after processing of the four groups, cells in each group were collected and stained using the Annexin-V FITC apoptosis detection kit according to the procedure given by the manufacturer. Flow cytometry was performed to analyse Annexin-V staining intensity and the procedure was repeated three times. For CLSM-based analysis of cell apoptosis, BT-474 cells were cultured in confocal culture dishes and processed as above in four groups, respectively. Thereafter, the cells were subjected to fixation using 4% paraformaldehyde and were covered by using the PI dye solution (5 μg/mL) for 5 min. After performing washing steps with PBS, the cells were observed via CLSM.

Animal Xenograft Models

After subjection to 2 days of sub-cutaneous implantation using 0.5 mg estradiol pellet, the breast cancer cells (BT-474) were injected into the right back area of athymic nude mice (5×10^6 cells per mouse). To construct HER2-positive model (5 weeks), HER2-negative cell MDA-MB-231 was cultured and injected to construct HER2-negative model (5×10^6 cells per mouse). The tumour volume was calculated by using the formula $V = (\pi \times A \times B \times C)/6$, where A, B, and C represent the length, width, and height diameters of the tumour, respectively. The diameters were measured using 2D ultrasound.

NIHA Complex Accumulation in Tumour and Distribution in vivo

The in vivo fluorescence imaging system (IVIS, Lumina II, Caliper, Boston, MA, USA) was used to visualise accumulation of the NIHA complex in the HER2-positive tumour. Briefly, 200 μL of the NIHA complex was injected in the caudal vein, and the HER2-positive mice were anaesthetised via inhalation of isopropyl fluoride with 1% concentration and were observed by using the IVIS system 12 h later. The Esaote MyLab Twice ultrasound diagnostic apparatus with a broad bandwidth (3–9 MHz) routine clinical linear array transducer (Esaote, LA522) was used to observe the tumour images before and after injection of the NIHA complex. After the mice were anaesthetised same as above, the ultrasound transducer was placed gently on the top of the tumour and the NIHA complex was injected. The imaging values were recorded, and the distribution and metabolism in nude mice was assessed. At 12, 24, 48, and 72

h after injection of 200 μL of the NIHA complex, the HER2-positive mice were sacrificed and the tumour, heart, liver, spleen, lung, kidney, and lymph were harvested and subsequently observed.

The Effect of NIHA Complex with Laser on Tumour in vivo

The mice were subjected to trials until the tumour volume reached an approximate value of 50 −100 mm^3. The mice were randomly separated into five groups as described following and 10 mice in each group: 1) the NIHA-laser HER2-positive group: 200 μL of the NIHA complex was injected into HER2-positive nude mice and laser was applied for 20 min; 2) the NIHA-laser HER2-negative group: 200 μL of the NIHA complex was injected into HER2-negative nude mice and laser was applied for 20 min; 3) the NIHA group: 200 μL of the NIHA complex was injected into HER2-positive nude mice without laser; 4) the laser group: the HER2-positive tumour on nude mice was subjected to irradiation by using laser for 20 min; 5) the control group: no processing was performed on HER2-positive nude mice. The tumour volume and cumulative survival were used to evaluate the effect on tumour in vivo. The tumour volume was measured once every 3 days after processing of the five groups. Moreover, the cumulative survival in the five groups was analysed via Kaplan–Meier survival analysis. Seventeen mice were killed by dislocation of the cervical vertebrae, and 33 mice were natural death. The tumour, heart, kidney, liver, spleen, and lung samples of five groups were separated to prepare paraffin-embedded sections. After deparaffinisation, haematoxylin and eosin (H&E) staining was performed and the sections were observed by using an optical microscope.

Statistical Analysis

All quantitative results are presented as mean ± SD (standard deviation). Statistical significance was determined with Student's *t*-test using SPSS software (v19.0; SPSS Inc., an IBM Company). The level of statistical significance was set at $P < 0.05$.

Results

Particle Size and Morphology

The particle size of the nanobubble-IR783-HPPH complex was approximately 444.6 ± 30.0 nm (n = 5) (Figure 2A). Moreover, after combining with affibody, the NIHA complex's particle size was 524.8 ± 53.3 nm (n = 5) (Figure 2B), PDI was −1.69 ± 0.83 and zeta potential was −31.98 ± 31.75mV (SFigure 1). The morphology of the NIHA complex was observed via TEM. The NIHA complex was observed as a spheroid with an uneven and unsmooth surface (Figure 2C). Based on the scale label in the figure, the particle size of the NIHA complex was <1000 nm. The NIHA complex assessed via CLSM is depicted as red dots with diameter <1000 nm (Figure 2D).

Stability and Cytotoxicity

The stability in particle size and the concentration of the NIHA complex were measured via DLS. The average particle sizes of the NIHA complex stored at 4 °C for 1 min, 30 min, 60 min, 6 h, and 24 h separately were 526.1 ± 47.8 nm (n = 5), 534.3 ± 61.9 nm (n = 5), 539.8 ± 69.4 nm (n = 5), 591.2 ± 62.4 nm (n = 5), and 647.4 ± 70.5 nm (n = 5), respectively (Figure 3A and SFigure 2A-E). Statistical analysis revealed a significant difference between the average particle size at 6 h and that at 1 min. The concentrations of the NIHA complex at same temperature and time as mentioned above were $(12.0 \pm 0.7) \times 10^6$ (n = 5), $(11.9 \pm 0.8) \times 10^6$ (n = 5), $(11.8 \pm 0.6) \times 10^6$ (n = 5), $(10.9 \pm 0.6) \times 10^6$ (n = 5), and $(10.1 \pm 0.7) \times 10^6$ (n = 5) (Figure 3B). The concentration at 6 h differed significantly from that observed at 1 min. The cytotoxicity of HPPH and IR783 were tested via CCK-8 assay. Figure 3C and D depict the cytotoxicity curve of HPPH and IR783, respectively. Statistical analysis revealed that remarkable cytotoxicity was detected when the concentration of HPPH increased to 20 μg/mL, and for IR783, it was 30 μg/mL.

Tumour Cell Targeting Capability

The ability of NIHA to target a specific cell was assessed via CLSM. As illustrated in Figure 4, the cell nucleus is observed and depicted as blue fluorescence in all groups. Meanwhile, red fluorescence was detected in the NIHA group and was not detected in the control group.

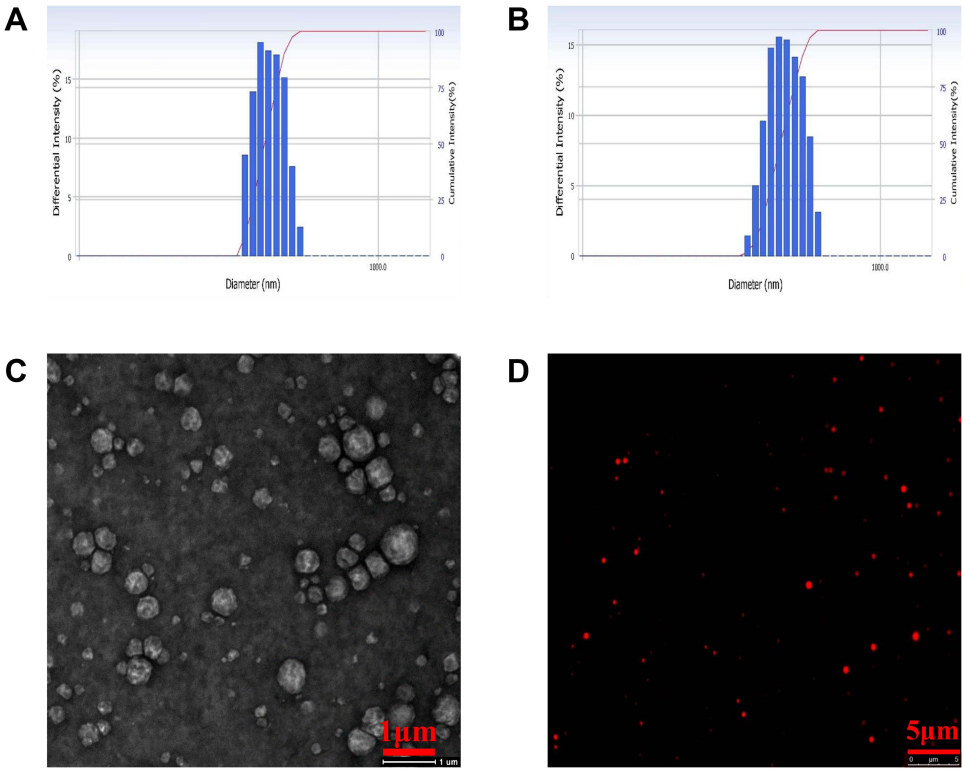

Figure 2 The particle size of the nanobubble-IR783-HPPH complex (**A**) and the NIHA complex (**B**). (**C**) The TEM results of the NIHA complex. (**D**) The fluorescence microscopy image of the NIHA complex.

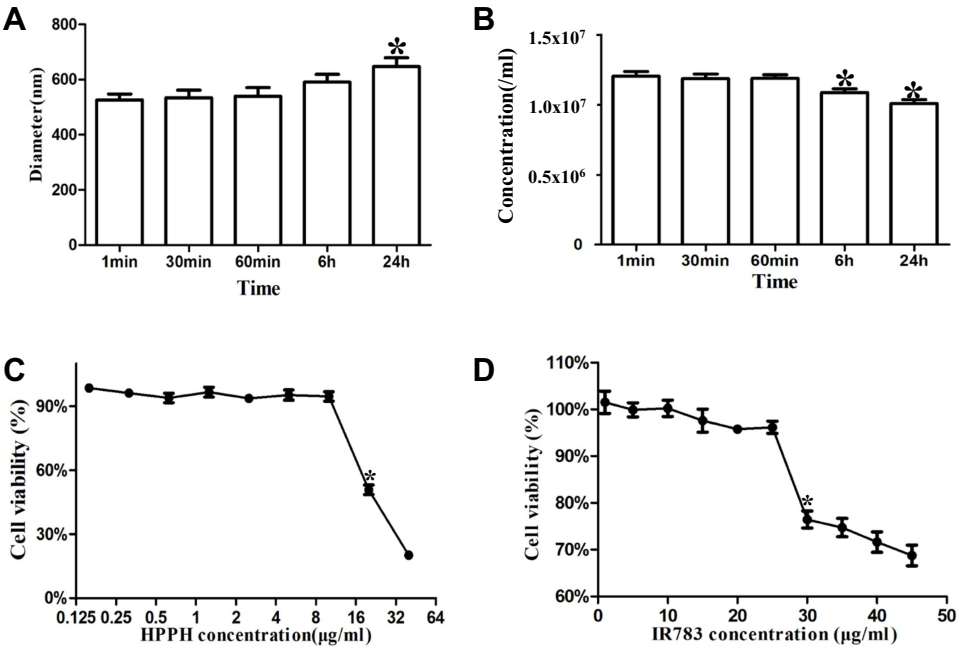

Figure 3 Stability and cytotoxicity. The diameter (**A**) and the concentration (**B**) stability of the NIHA complex at 4 °C (*P < 0.05 indicated statistically significant differences compared with those observed at 1 min). In vitro cytotoxicity for various concentrations of HPPH (**C**) and IR783 (**D**) determined by using the CCK-8 assay (*P < 0.05 indicates statistically significant differences compared with normal cells).

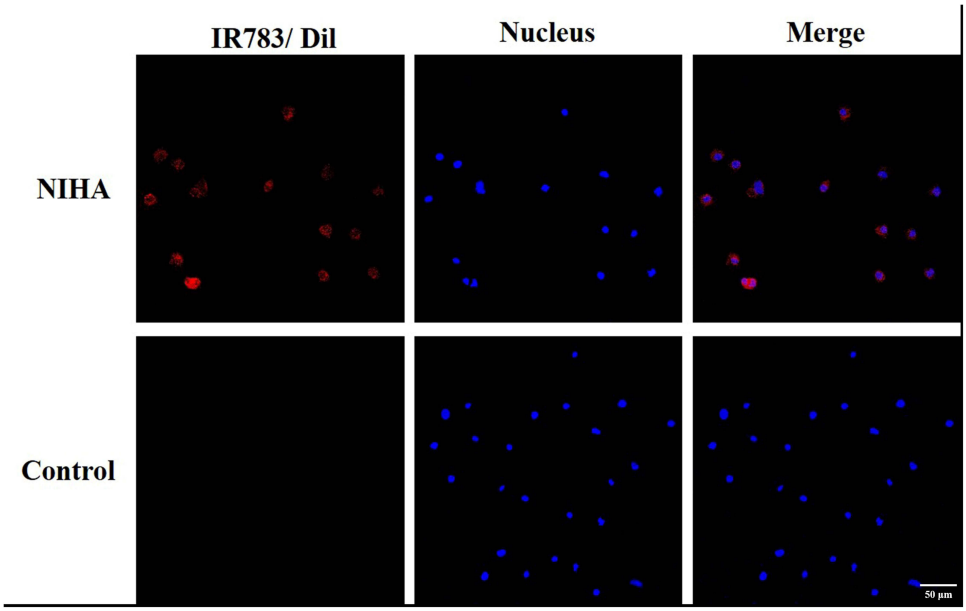

Figure 4 The targeting ability of the NIHA complex. The CLSM images of BT-474 cells incubated with the NIHA complex (up) and the nanobubble-Dil-HPPH complex (down). Bar, 50 μm.

The Effect of NIHA Complex with Laser on Cell in vitro

Cell viability and apoptosis were determined to evaluate. The cell viability analysis via CCK-8 assay indicated that the NIHA-laser group exhibited viability of 9.86% ± 10.86%. Moreover, the NIHA, laser, and control groups exhibited viabilities of 95.59% ± 12.29%, 98.82% ± 7.84%, and 100.00% ± 8.89%, respectively. Compared with the other three groups, the NIHA-laser group exhibited the lowest rate of viability (Figure 5A). Cell apoptosis was assessed via flow cytometry and CLSM. As illustrated in Figure 5B and SFigure 3, the BT-474 cell apoptosis rate in the NIHA-laser group was 84.56% ± 4.30%, which was higher than that in the NIHA (5.06% ± 1.99%), laser (0.42% ± 0.20%), and control (0.46% ± 0.26%) groups, respectively. In the NIHA-laser group, red fluorescence was observed around the BT-474 cells. Furthermore, red fluorescence was slightly detected in the NIHA group and no fluorescence was observed in the laser and control groups. The cell structures in the other three groups were complete and were clearer (Figure 6).

Accumulation of NIHA in Tumour Tissues

The NIHA complex was injected into the tail vein of nude mice bearing tumour tissues, and the NIRF images of mice were observed. Figure 7A illustrates remarkable fluorescence in the tumour tissue, thereby indicating accumulation of the

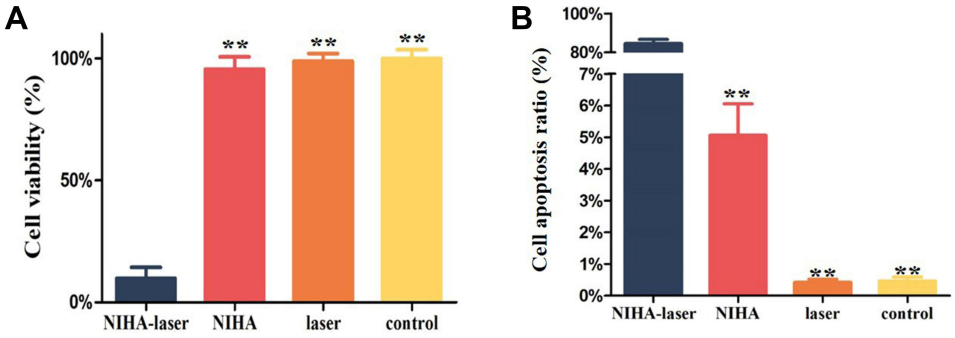

Figure 5 (**A**) Cell viability of BT-474 cells detected via CCK-8. (**B**) The apoptotic ratio of BT-474 cells detected via Annexin-V flow cytometry. $^{**}P < 0.01$ compared with the NIHA-laser group.

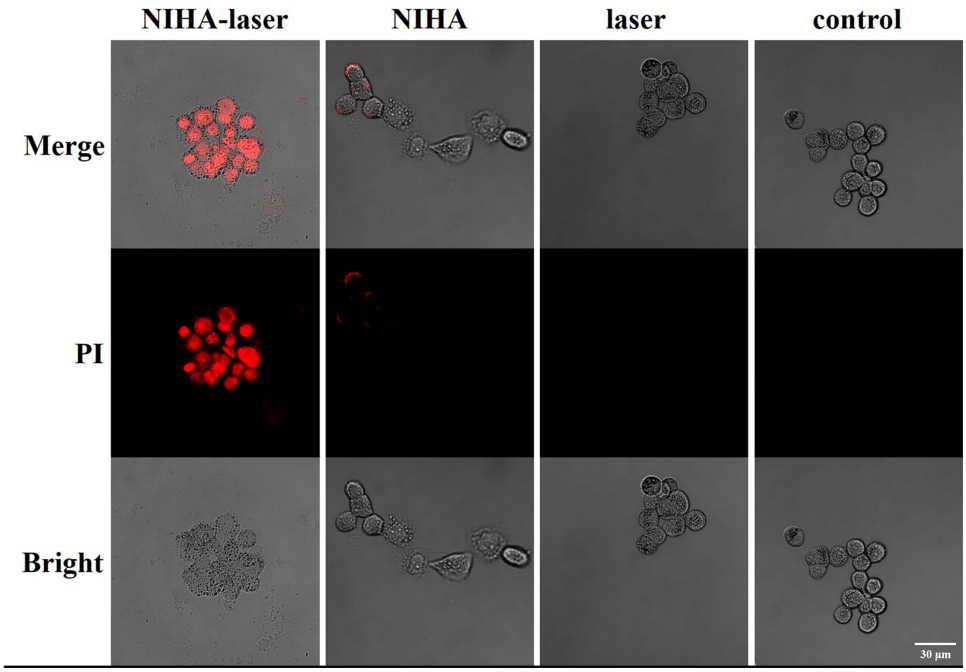

Figure 6 CLSM images of BT-474 cells in the NIHA-laser, NIHA, laser, and the control groups. The nuclei of the apoptosis cells were stained by using PI (depicted as red fluorescence). Bar, 30 μm.

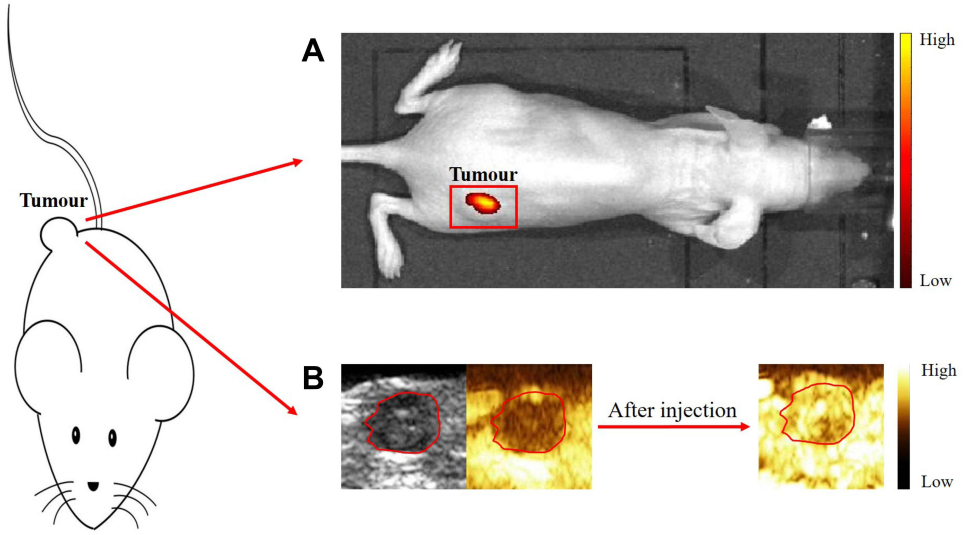

Figure 7 (**A**) The NIRF imaging of xenografts in nude mice after injection of the NIHA complex. (**B**) The ultrasound contrast-enhanced imaging of xenografts in nude mice before and after injection of the NIHA complex.

NIHA complex. B-mode and contrast-enhanced model ultrasound were performed to observe the tumour directly. After injection, imaging contrast enhancement was observed in the contrast-enhanced model (Figure 7B).

NIHA Distribution and Metabolism

To further confirm the distribution and metabolism of NIHA complex in vivo, a tissue fluorescence imaging experiment was conducted. Fluorescent signals derived from the tumour, heart, liver, spleen, lung, kidney, and lymph of nude mice were analysed at different time points after injection (Figure 8). The fluorescence signal was detected in the tumour, liver, lung, and kidney, whereas only mild signal was observed in the heart, spleen, and lymph. The fluorescence intensity of

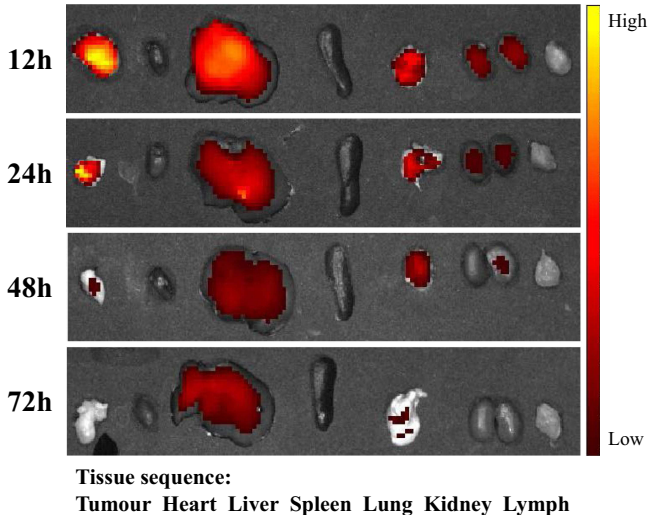

Figure 8 In vitro fluorescence imaging of the tumour, heart, liver, spleen, lung, kidney, and lymph at different time points after NIHA complex injection.

tumour, liver, lung, and kidney gradually decreased with time. Furthermore, the strongest fluorescence intensity was observed in the tumour at 12 and 24 h, in the lung at 48 h, and in the liver at 72 h.

The Effect of NIHA Complex with Laser on Tumour in vivo

To evaluate the effect of NIHA with laser, the tumour volume growth was recorded and analysed, and the results have been illustrated in Figure 9A. The tumour volume of NIHA, laser, and control groups gradually increased with time; however, that of the NIHA-laser HER2-positive group and the NIHA-laser HER2-negative group gradually decreased and the NIHA-laser HER2-positive group was more obvious. The cumulative survival (Figure 9B) revealed that the nude mice in the NIHA-laser HER2-positive, the NIHA-laser HER2-negative group, NIHA, laser, and control groups gradually succumbed on days 55, 57, 50, 44, and 48, respectively. Kaplan–Meier survival analysis showed that the NIHA-laser HER2-positive group had a longer survival ($P < 0.05$) compared to NIHA, laser, and control groups, and no statistical difference with the NIHA-laser HER2-negative group ($P = 0.417$). However, the NIHA-laser HER2-positive group exhibited a higher survival percentage on day 80 when all the nude mice in the control group died.

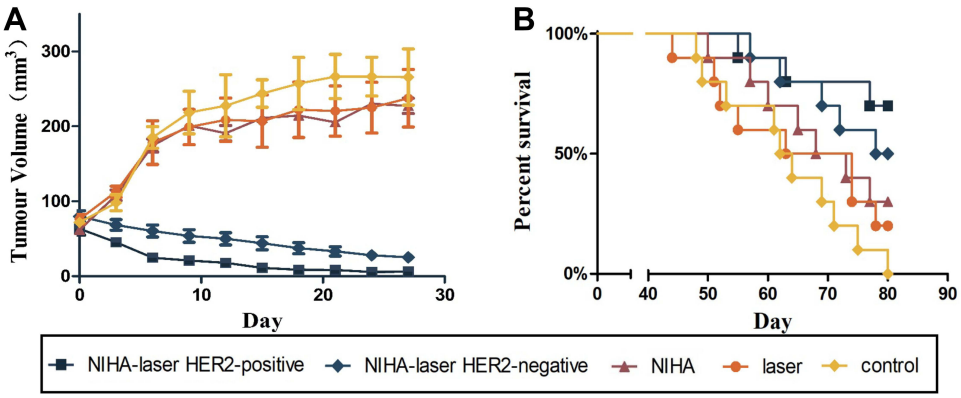

Figure 9 Tumour growth inhibition and cumulative survival of mice assessed in various treatment groups. (**A**) Tumour volume growth of each group. (**B**) The cumulative survival of mice in each group.

Pathology

The histological changes in each group were observed via H&E staining (Figure 10). The tumour tissue of the NIHA-laser HER2-positive group revealed fewer cells and lower levels of polymorphism, in contrast to the other four groups. Meanwhile, no significant alterations were observed in the heart, kidney, liver, spleen, and lung among the four groups.

Discussion

As breast cancer is the most commonly reported tumour in females, its treatment has gained considerable attention in research, particularly in the case of HER2-positive breast cancer, which predicts a poor prognosis and high mortality.[3,4] Although conventional cancer therapies such as surgery, chemotherapy, immunotherapy, radiation, and others have been markedly explored, certain issues such as surgical injury and side effects persist. The appearance of NB provides a new approach for targeted imaging and treatment of the tumour. NB can pass through the tumour blood vessel, accumulate in the intercellular space, and connect with ligand would improve its targeting ability. Therefore, based on protocols reported in our previous studies, we fabricated the NIHA complex and used it in combination with laser treatment to inhibit tumour growth and to treat breast cancer.

The NIHA complex was fabricated by adopting the thin-film hydration method and its characteristics were detected. The particle size measured by DLS confirmed that the size of the nanobubble-IR783-HPPH complex was in the nanometre range. After conducting linkage of the affibody by using the biotin–streptavidin system, the NIHA complex was examined and findings revealed a similar particle size to the nanobubble-IR783-HPPH complex, which affirmed that the operation could not affect the particle size markedly and the diameter of the NIHA complex satisfied the requirement

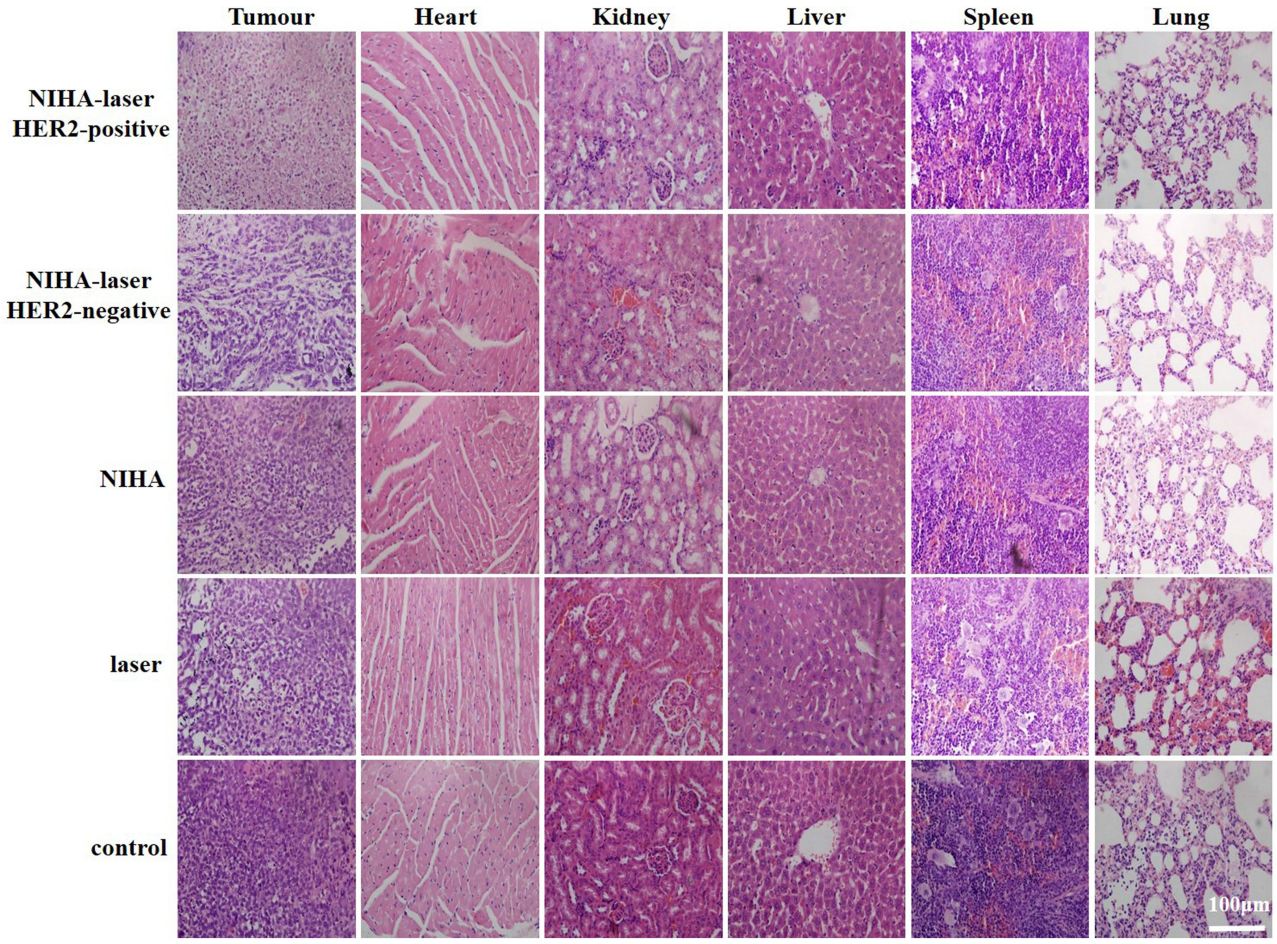

Figure 10 H&E assay performed for the sections of tumour, heart, kidney, liver, spleen, and lung in the five different groups. Bar, 100 μm.

of subsequent experiments. Through the results of TEM and CLSM, we confirmed the spherical morphology of the NIHA complex, and findings on its diameter were consistent with the DLS results. The stability results indicated that the particle size and the concentration of the NIHA complex were relatively stable at 4 °C and differed significantly at 24 and 6 h after fabrication, respectively. Its relative stability is partly attributable to the gaseous core C_3F_8 which is stable and exhibits low dispersion and blood solubility.[27] The concentration of IR783 and HPPH, at which their cytotoxicity was observed, in all experiments was significantly less than 30 and 20 μg/mL, respectively. The cytotoxicity of phospholipid DPPC and DSPE-PEG (2000) were investigated in our previous studies.[25,28] Moreover, due to their hypo-cytotoxicity, DPPC and DSPE-PEG (2000) have been used to fabricate MB and NB in several studies.[23,24,29,30] Therefore, fabrication materials of the NIHA complex would not lead to cell apoptosis or decreased viability. In the tumour targeting test, compared to the control group, red fluorescence was detected around the cell nucleus (exhibiting blue fluorescence) in the NIHA group, which indicated that NIHA complex exhibited the HER2 cancer cell targeting capability, and without the presence of affibody and IR783 (control group), it could not establish connection with the cell.

We assumed that the NIHA complex used in combination with laser treatment would inhibit the growth of tumour cells and induce their apoptosis, and this was evaluated via CCK-8 assay, flow cytometry, and CLSM. The NIHA-laser group exhibited higher apoptosis and lower cell viability, compared with the other three groups. In the CLSM results, the NIHA-laser group revealed an increase in red fluorescence, which indicated a better effect in vitro. This is mainly because HPPH is a second-generation photosensitizer of PDT, which can help generate ROS under light irradiation conditions to inflict irreversible damage on the tumour cells.[31] Hence, neither HPPH (the NIHA group) nor laser (the laser group) treatment alone can achieve such an effect.

After the performance of caudal vein injection, the signal intensity of fluorescent and contrast-enhanced ultrasound observed via IVIS and ultrasound increased only in the tumour tissue, which confirmed the accumulation of the NIHA complex in the tumour tissue. Tissue fluorescence imaging was conducted to observe the distribution and metabolism of the NIHA complex, which mainly focused on examination of the characteristics of the tumour tissue. In accordance with the findings reported in previous studies, it was observed that a considerable portion of MB and NB was cleared by the hepatic system,[28,32] which was consistent with the findings obtained in the present study.

In the in vivo experiments, the NIHA group and the laser group demonstrated that without laser or NIHA treatment, the inhibition efficacy of tumour was reduced. In contrast to the three four groups, the NIHA-laser HER2-positive group and the NIHA-laser HER2-negative group markedly inhibited the tumour volume, prolonged nude mice survival, but the former one was more pronounced. Moreover, organs such as the liver, kidney, heart, and others did not reveal any significant changes. This may presumably be attributable to the following three major reasons: (1) the non-toxicity of the NIHA complex. The NIHA complex comprises DDPC, DSPE-PEG (2000), C_3F_8 gas, affibody, HPPH, and IR783. The first four were widely applied in various studies and their safety was verified. The cytotoxicity of HPPH and IR783, as discussed above, was lower than the concentration at which evident cytotoxicity was observed; (2) the tumour targeting ability of the NIHA complex. The majority of tumour vessels demonstrate a pore cutoff size ranging from 380 to 780 nm.[33,34] Considering its particle size, the NIHA complex can penetrate through gaps of inter-endothelial tumour and is markedly large for normal tissues whose inter-endothelial gaps are less than 7 nm.[35] The presence of affibody and IR783 enhanced the tumour targeting ability of the NIHA complex; (3) light irradiation in specific area. The position of laser irradiation can be controlled in the tumour tissue, which may help reduce its influence on normal tissues. Hence, the NIHA-laser group showed marked inhibition of the tumour tissue but rarely showed effects in normal tissues.

Conclusion

In summary, we fabricated the NB-IR783-HPPH complex by adopting an advanced thin-film hydration method and further enabled the establishment of connections with HER2 affibody by using the avidin–biotin system to facilitate the formation of the NIHA complex. The complex exhibits a good particle size, stability, and no evident cytotoxicity. In the in vitro experiments, it exhibited the ability of targeting HER2-positive breast cancer cells, inhibited the growth of tumour cells, and induced their apoptosis. Furthermore, due to its nanoscale size and presence of affibody and IR783, the NIHA complex could accumulate in the tumour tissue and could suppress tumour growth when used in conjunction with laser treatment in vivo. Hence, the NIHA complex could be used as an innovative, non-invasive therapeutic tool for

HER2-positive breast cancer with low side effects. Furthermore, the NIHA complex's real time in vivo biodistribution and longtime preservation should be studied in the future.

Abbreviations

CLSM, confocal laser scanning microscope; DLS, dynamic light scattering; DMEM, the Dulbecco's modified Eagle medium; FBS, fetal bovine serum; NIHA, nanobubble-IR783-HPPH-affibody; HER2, human epidermal growth factor receptor 2; NB, nanobubble; MB, microbubble; EPR, the enhanced permeability and retention; PDI, polydispersity index; PDT, photodynamic therapy; ROS, reactive oxygen species; HPPH, 2-[1-hexyloxyethyl]-2-devinyl pyropheophorbide-a; PBS, phosphate-buffered saline; TEM, transmission electron microscope.

Data Sharing Statement

All data generated or analysed during this study are included in this published article and its supplementary information file.

Ethics Approval and Consent to Participate

All experimental protocols were approved by the ethic committee of Tangdu hospital Fourth Military Medical University. All the methods and animal care methods were carried at the Fourth Military Medical University on Animal Care and Use in accordance with the National Institutes of Health (NIH) guidelines. All methods are reported in accordance with ARRIVE guidelines.

Author Contributions

All authors made a significant contribution to the work reported, whether that is in the conception, study design, execution, acquisition of data, analysis and interpretation, or in all these areas; took part in drafting, revising or critically reviewing the article; gave final approval of the version to be published; have agreed on the journal to which the article has been submitted; and agree to be accountable for all aspects of the work.

Funding

This study was financially supported by the National Natural Science Foundation of China (Grant no. 81571730).

Disclosure

The authors declare that they have no competing interests in this work.

References

1. Bray F, Ferlay J, Soerjomataram I, Siegel RL, Torre LA, Jemal A. Global cancer statistics 2018: GLOBOCAN estimates of incidence and mortality worldwide for 36 cancers in 185 countries. *CA Cancer J Clin*. 2018;68(6):394–424. doi:10.3322/caac.21492
2. Waks AG, Winer EP. Breast cancer treatment: a review. *JAMA*. 2019;321(3):288–300. doi:10.1001/jama.2018.19323
3. Chen CY, Yang CY, Chen YC, Shih CW, Lo SS, Lin CH. Decreased expression of stomatin predicts poor prognosis in HER2-positive breast cancer. *BMC Cancer*. 2016;16:697. doi:10.1186/s12885-016-2681-7
4. Gianni L, Pienkowski T, Im YH, et al. Efficacy and safety of neoadjuvant pertuzumab and trastuzumab in women with locally advanced, inflammatory, or early HER2-positive breast cancer (NeoSphere): a randomised multicentre, open-label, Phase 2 trial. *Lancet Oncol*. 2012;13(1):25–32. doi:10.1016/S1470-2045(11)70336-9
5. Menendez JA, Papadimitropoulou A, Vander Steen T, et al. Fatty acid synthase confers tamoxifen resistance to ER+/HER2+ breast cancer. *Cancers*. 2021;13(5):1132. doi:10.3390/cancers13051132
6. Yin L, Wang ZY. Roles of the ER-alpha 36-EGFR/HER2 positive regulatory loops in tamoxifen resistance. *Steroids*. 2016;111:95–99. doi:10.1016/j.steroids.2016.01.019
7. Musolino A, Ciccolallo L, Panebianco M, et al. Multifactorial central nervous system recurrence susceptibility in patients with HER2-positive breast cancer: epidemiological and clinical data from a population-based cancer registry study. *Cancer*. 2011;117(9):1837–1846. doi:10.1002/cncr.25771
8. Hyman DM. Vemurafenib in multiple nonmelanoma cancers with BRAF V600 mutations; adjuvant pertuzumab and trastuzumab in early HER2-positive breast cancer. *N Engl J Med*. 2018;379(16):1585. doi:10.1056/NEJMx180036
9. Dieras V, Miles D, Verma S, et al. Trastuzumab emtansine versus capecitabine plus lapatinib in patients with previously treated HER2-positive advanced breast cancer (EMILIA): a descriptive analysis of final overall survival results from a randomised, open-label, Phase 3 trial. *Lancet Oncol*. 2017;18(6):732–742. doi:10.1016/S1470-2045(17)30312-1

10. Musolino A, Boggiani D, Pellegrino B, et al. Role of innate and adaptive immunity in the efficacy of anti-HER2 monoclonal antibodies for HER2-positive breast cancer. *Crit Rev Oncol Hematol*. 2020;149:102927. doi:10.1016/j.critrevonc.2020.102927
11. Agostinis P, Berg K, Cengel KA, et al. Photodynamic therapy of cancer: an update. *CA Cancer J Clin*. 2011;61(4):250–281. doi:10.3322/caac.20114
12. Hopper C. Photodynamic therapy: a clinical reality in the treatment of cancer. *Lancet Oncol*. 2000;1:212–219. doi:10.1016/S1470-2045(00)00166-2
13. Dobson J, de Queiroz GF, Golding JP. Photodynamic therapy and diagnosis: principles and comparative aspects. *Vet J*. 2018;233:8–18. doi:10.1016/j.tvjl.2017.11.012
14. Saenz C, Cheruku RR, Ohulchanskyy TY, et al. Structural and epimeric isomers of HPPH [3-devinyl 3-{1-(1-hexyloxy) ethyl}pyropheophorbide-a]: effects on uptake and photodynamic therapy of cancer. *ACS Chem Biol*. 2017;12(4):933–946. doi:10.1021/acschembio.7b00023
15. Bellnier DA, Greco WR, Nava H, Loewen GM, Oseroff AR, Dougherty TJ. Mild skin photosensitivity in cancer patients following injection of Photochlor (2-[1-hexyloxyethyl]-2-devinyl pyropheophorbide-a; HPPH) for photodynamic therapy. *Cancer Chemother Pharmacol*. 2006;57(1):40–45. doi:10.1007/s00280-005-0015-6
16. Bellnier DA, Greco WR, Loewen GM, et al. Population pharmacokinetics of the photodynamic therapy agent 2-[1-hexyloxyethyl]-2-devinyl pyropheophorbide-a in cancer patients. *Cancer Res*. 2003;63(8):1806–1813.
17. Fang J, Nakamura H, Maeda H. The EPR effect: unique features of tumor blood vessels for drug delivery, factors involved, and limitations and augmentation of the effect. *Adv Drug Deliv Rev*. 2011;63(3):136–151. doi:10.1016/j.addr.2010.04.009
18. Franco MS, Gomes ER, Roque MC, Oliveira MC. Triggered drug release from liposomes: exploiting the outer and inner tumor environment. *Front Oncol*. 2021;11:623760. doi:10.3389/fonc.2021.623760
19. Dai J, Zou S, Pei Y, Cheng D, Ai H, Shuai X. Polyethylenimine-grafted copolymer of poly(l-lysine) and poly(ethylene glycol) for gene delivery. *Biomaterials*. 2011;32(6):1694–1705. doi:10.1016/j.biomaterials.2010.10.044
20. Yang X, Zhu B, Dong T, Pan P, Shuai X, Inoue Y. Interactions between an anticancer drug and polymeric micelles based on biodegradable polyesters. *Macromol Biosci*. 2008;8(12):1116–1125. doi:10.1002/mabi.200800085
21. Prabhakar A, Banerjee R. Nanobubble liposome complexes for diagnostic imaging and ultrasound-triggered drug delivery in cancers: a theranostic approach. *ACS Omega*. 2019;4(13):15567–15580. doi:10.1021/acsomega.9b01924
22. Wu H, Rognin NG, Krupka TM, et al. Acoustic characterization and pharmacokinetic analyses of new nanobubble ultrasound contrast agents. *Ultrasound Med Biol*. 2013;39(11):2137–2146. doi:10.1016/j.ultrasmedbio.2013.05.007
23. Yang H, Cai W, Xu L, et al. Nanobubble-Affibody: novel ultrasound contrast agents for targeted molecular ultrasound imaging of tumor. *Biomaterials*. 2015;37:279–288. doi:10.1016/j.biomaterials.2014.10.013
24. Lv W, Shen Y, Yang H, et al. Imaging agent targeting HER2 molecule of breast cancer. *J Immunol Res*. 2018;2018:6202876. doi:10.1155/2018/6202876
25. Cai WB, Yang HL, Zhang J, et al. The optimized fabrication of nanobubbles as ultrasound contrast agents for tumor imaging. *Sci Rep*. 2015;5:13725. doi:10.1038/srep13725
26. Yano S, Hirohara S, Obata M, et al. Current states and future views in photodynamic therapy. *J Photochem Photobiol C*. 2011;12(1):46–67. doi:10.1016/j.jphotochemrev.2011.06.001
27. Abou-Elkacem L, Bachawal SV, Willmann JK. Ultrasound molecular imaging: moving toward clinical translation. *Eur J Radiol*. 2015;84(9):1685–1693. doi:10.1016/j.ejrad.2015.03.016
28. Cai W, Lv W, Feng Y, et al. The therapeutic effect in gliomas of nanobubbles carrying siRNA combined with ultrasound-targeted destruction. *Int J Nanomedicine*. 2018;13:6791–6807. doi:10.2147/IJN.S164760
29. Zhou T, Cai W, Yang H, et al. Annexin V conjugated nanobubbles: a novel ultrasound contrast agent for in vivo assessment of the apoptotic response in cancer therapy. *J Control Release*. 2018;276:113–124. doi:10.1016/j.jconrel.2018.03.008
30. Yin T, Wang P, Li J, et al. Tumor-penetrating codelivery of siRNA and paclitaxel with ultrasound-responsive nanobubbles hetero-assembled from polymeric micelles and liposomes. *Biomaterials*. 2014;35(22):5932–5943. doi:10.1016/j.biomaterials.2014.03.072
31. Wang Z, Zhang F, Shao D, et al. Janus nanobullets combine photodynamic therapy and magnetic hyperthermia to potentiate synergetic anti-metastatic immunotherapy. *Adv Sci*. 2019;6(22):1901690. doi:10.1002/advs.201901690
32. Willmann JK, Cheng Z, Davis C, et al. Targeted microbubbles for imaging tumor angiogenesis: assessment of whole-body biodistribution with dynamic micro-PET in mice. *Radiology*. 2008;249(1):212–219. doi:10.1148/radiol.2491072050
33. Hobbs SK, Monsky WL, Yuan F, et al. Regulation of transport pathways in tumor vessels: role of tumor type and microenvironment. *Proc Natl Acad Sci U S A*. 1998;95(8):4607–4612. doi:10.1073/pnas.95.8.4607
34. Oeffinger BE, Wheatley MA. Development and characterization of a nano-scale contrast agent. *Ultrasonics*. 2004;42(1–9):343–347. doi:10.1016/j.ultras.2003.11.011
35. Rapoport NY, Nam KH, Gao Z, Kennedy A. Application of ultrasound for targeted nanotherapy of malignant tumors. *Acoust Phys*. 2009;55(4–5):594–601. doi:10.1134/S1063771009040162